

Numerical investigation into the Nd doped YAG rod grooving impact on the sunlight-pumped-laser performance

M. Said^{a,b}, H. Noureddine^{a,b}, and F. Rehouma^{a,b}

^a*Departement of physics, University of El Oued, El Oued 39000, Algeria.*

^b*LEVRES laboratory, University of El Oued, El Oued 39000, Algeria.*

Received 14 December 2023; accepted 9 February 2024

This paper presents a numerical analysis of the impact of grooving the Nd doped YAG rod on the sunlight-pumped lasers performance. The study analyzes laser systems that utilize side-exciting and end-side-exciting approaches to activate both grooved and non-grooved Nd doped YAG laser rods. The effects of the rod surface groove on the performance of the sunlight-pumped-lasers are thoroughly examined using ZEMAX[©] and LASCAD[©] softwares. To excite the grooved and non-grooved Nd doped YAG rods alternately, a ring-array sunlight flux concentrator is employed. Moreover, in the side-exciting technique, the head of the laser system contains a rectangular light guide of an extremely transparent glass made from fusing silica and an excitation cavity with a V-shaped configuration, housing the Nd doped YAG rod. This exciting method with a grooved laser rod resulted in a 13.70% increase in laser power and a 28.20% reduction in stress intensity compared to the non-grooved rod. In the end-side-exciting technique, the head of the laser system comprises an aspheric lens made of a fused silica glass and a conical-shaped excitation cavity, accommodating the Nd doped YAG rod. Results indicate that using grooved laser rod in this exciting system did not lead to an amelioration in output laser power. However, this technique enhanced the stress intensity by a reduction of 35.03%.

Keywords: Sunlight-pumped-laser; ring-array sunlight flux concentrator; grooved laser rod; end-exciting method; side-exciting configuration.

DOI: <https://doi.org/10.31349/RevMexFis.70.041301>

1. Introduction

Systems of sunlight-pumped laser have emerged as a full of promise technology altering sunlight directly into laser light. It provides a vast range of uses in both terrestrial and space fields. The first research on sunlight-pumped lasers was conducted by Kiss *et al.* and C. G. Young in the early 1960s [1,2]. Since then, several researchers have contributed to the improvement of sunlight-pumped laser systems, including Arashi *et al.* [3], Weskler *et al.* [4], Vasylyev *et al.* [5], Lando *et al.* [6,7], Zhao, *et al.* [8], Saiki *et al.* [9], Yabe *et al.* [10], Ohkubo, *et al.* [11], Dinh *et al.* [12], Xu *et al.* [13], Payziyev *et al.* [14-16], Bouadjemine *et al.* [17], Mehellou *et al.* [18,19], Guan *et al.* [20, 21], Masuda *et al.* [22], Liang *et al.* [23-35], Almeida *et al.* [36-43], Vistas *et al.* [44-52], Garcia *et al.* [53-58], Matos *et al.* [59], Tibúrcio *et al.* [60-65], Costa *et al.* [66,71], Boutaka *et al.* [72], Catela *et al.* [73-78], Berwal *et al.* [79], Cai *et al.* [80], who have made significant progress in enhancing the performance of sunlight-pumped lasers.

Sunlight-pumped laser systems operate by collecting, concentrating, homogenizing and distributing the solar radiation, afterwards, compressed into, or wrapped around, the active medium. Two commonly employed techniques for activating the laser medium are end-side-exciting and side-exciting. While end-side-exciting is known for its efficiency, it often leads to thermal loading issues caused by the concentration of absorbed excitation light at the end of the laser rod. Side-exciting, on the other hand, offers regular distribu-

tion of the exciting light inside the laser rod but is relatively less efficient compared to end-side exciting [81]. To enhance the efficiency of side-exciting, grooved laser rods have been proposed. The grooved surfaces minimize optical reflection losses and provide a larger interface with cooling liquid, facilitating improved heat dissipation [13,44].

Sunlight-pumped lasers have utilized grooved Nd doped YAG laser rods in various experiments (Table I recapitulates the main research in which this kind of rods have been employed).

The absorption and distribution of exciting light within the laser medium play a decisive role in the efficiency of sunlight-pumped lasers. Therefore, optimizing sunlight-pumped laser systems requires careful consideration of these factors. While non-grooved rods are more commonly used, grooved rods offer improved absorption of exciting light when utilizing the side-pumping configuration.

Given the potential of grooved rods as laser medium in side-sunlight-pumped lasers, it is essential to investigate the impact of grooved surfaces on the performance of these systems. Consequently, the focus of this study is to inspect the influence of rod grooved surfaces on the output performance of sunlight-pumped lasers. Although both types of rods have been employed in sunlight-pumped lasers, there is currently no comparative study evaluating their effects on the performance of these systems.

TABLE I. Main research in which the grooved rods have been employed.

Primary concentrator		Secondary concentrator	Pumping		Active medium		Laser power (W)	Collection efficiency (W/m ²)	Laser beam brightness (W)	
Source	Kind, collection area		Cavity	Method	Type					
					Diameter (mm)	Length (mm)				
P. Xu <i>et al.</i> , 2014, [13]	Fresnel lens, (1.3 m ²)	—	Ceramic conical cavity	End side	Grooved Nd : YAG		20.3	15.61	—	
		Water tube lens	Copper conical cavity		6.0	100	27	20.80	—	
C. R. Vistas <i>et al.</i> , 2015, [44]	Parabolic mirror, (3.14 m ²)	Silica semi-cylindrical lens	2V-shaped cavity	side-	Grooved Nd : YAG	Num.	8.5	17.1		
						TEM ₀₀ 25.5				
					3.5	34	Exp.	TEM ₀₀ 4.0	3.1	3.0
Z. Guan <i>et al.</i> , 2016, [20]	Fresnel lens, (1.3 m ²)	Water tube lens	Conical cavity	End-side-	Grooved Nd : YAG		31.95	31	—	
					6.0	95				
C. R. Vistas <i>et al.</i> , 2016, [45]	Parabolic mirror, (1.0 m ²)	Silica tube lens	2V-shaped cavity	side-	Grooved Nd : YAG		TEM ₀₀ 3.4	3.4	—	
					4.0	34				
C. R. Vistas <i>et al.</i> , 2020, [48]	Parabolic mirror, (3.14 m ²)	Rectangular hollow pipe	2V-shaped cavity	side-	Grooved Nd : YAG		TEM ₀₀ 32	10.7	31.4	
					4.5	34				
C. R. Vistas <i>et al.</i> , 2016, [45]	Parabolic mirror, (1.0 m ²)	Silica tube lens	2V-shaped cavity	side-	Grooved Nd : YAG		TEM ₀₀ 3.4	3.4	—	
					4.0	34				
H. Costa <i>et al.</i> , 2023, [71]	Six Fresnel lens, (Total collection 10 m ²)	Six fused silica aspheric lenses and rectangular CPCs	Cylindrical cavity	side-	Seven grooved Nd : YAG		TEM ₀₀ 153.29	15.33	Conversion efficiencies	
					2.7	35			1.61%	

To address this gap, a sunlight-pumped laser system composed of a stage for solar radiation collection and concentration using a ring-array sunlight flux concentrator (RAC) described by Garcia *et al.* [54] is exploited. The RAC is utilized to side-exciting and end-side-exciting a grooved and a non-grooved Nd doped YAG rods, respectively. In the side-

exciting technique, the laser rod is activated through a rectangular light guide of an extremely transparent glass made from fusing silica and a 3V-shaped excitation cavity, while in the end-side-exciting approach, an aspheric lens made of a fused silica glass and a conical-shaped excitation cavity are used to excite the Nd doped YAG rod.

TABLE II. Parameters of the elements constituting the RAC (Rings and Fresnel lens).

Reflective ring (from great to small)	Ring 1	Ring 2	Ring 3	Ring 4	Ring 5	Ring 6	Ring 7	Fresnel lens
Maximum aperture (mm)	500	470	420.84	352.33	272.62	197.08	136.45	92.37
Minimum aperture (mm)	470	420.84	352.33	272.62	197.08	136.45	92.37	0.00
Radius of curvature (mm)	282.35	237.07	177.88	115.19	64.28	31.99	14.84	208.13
Vertical distance between the minimum aperture and the focal plane (mm)	250.00	255.00	260.00	265.00	270.00	275.00	280.00	413.27

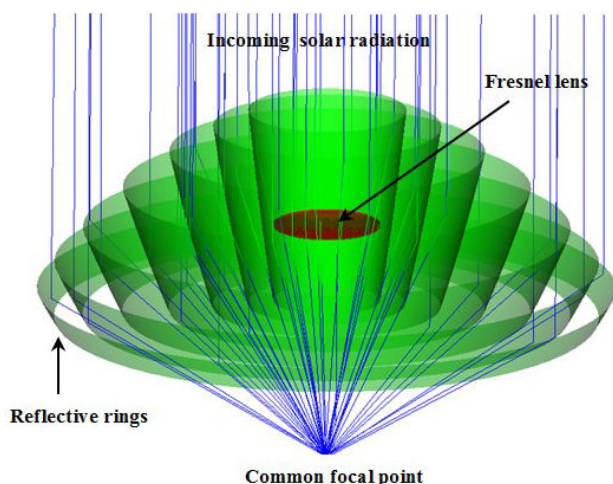


FIGURE 1. RAC designed by seven rings and a Fresnel lens.

2. Ring-array sunlight flux collector and concentrator system

Figure 1 illustrates a ring-array sunlight flux concentrator system consisting of seven rings, each with unique diameters and radii of curvature. All the rings adopt a profile of an off-axis parabolic and have a reflectivity of 95%. To maximize the utilization of the collection surface, a little Fresnel lens is sited at the RAC central zone.

The reflective ring with a diameter of 1.0 m creates 0.785 m² collection area. Given an average of 950 W/m² solar irradiance, the system is capable to concentrate 745.75 W sun light power into a spot of a full-width of a 5 mm at half

maximum diameter and a profile of a near-Gaussian aspect. This spot is located 250 mm in relation to the center of the minimum aperture of the large ring, as depicted in Fig. 2. To complete the description of the ring-array concentrator system, its parameters are summarized in Table II.

3. Sunlight-pumped laser exiting system

Typically, the exciting process is conducted using two main methods, namely side-exciting and end-side-exciting techniques.

3.1. Side-Exciting method

The side-exciting setup offers several advantages, such as enabling uniform absorption distribution throughout the length of the laser rod, conducting to a laser beam of high quality. However, this configuration typically exhibits a relatively lower efficiency in transferring solar energy to laser light liken to the end-side-exciting technique. One method to enhance the efficiency of side-pumping is to use a grooved laser rod. To demonstrate the effectiveness of the grooved laser rod, a comparative analysis will be conducted to evaluate the performance of non-grooved and grooved laser rods.

3.2. Sunlight-pumped laser head

Figure 3 illustrates the laser head composition, which includes a rectangular light guide of an extremely transparent glass made from fusing silica and an excitation cavity with a V-shaped configuration, housing the Nd doped YAG rod.

TABLE III. Dimensions of the laser head components.

Elements						
Light guide of fused silica		V-shaped excitation cavity		Nd doped YAG		
Dimensions	Values	Dimensions	Values	Dimensions	Values	
Cross section (mm)	(22 × 14)	Angle (°)	V ₁	11	Diameter (mm)	4
			V ₂	23		
Length (mm)	50		V ₃	45	Length (mm)	30

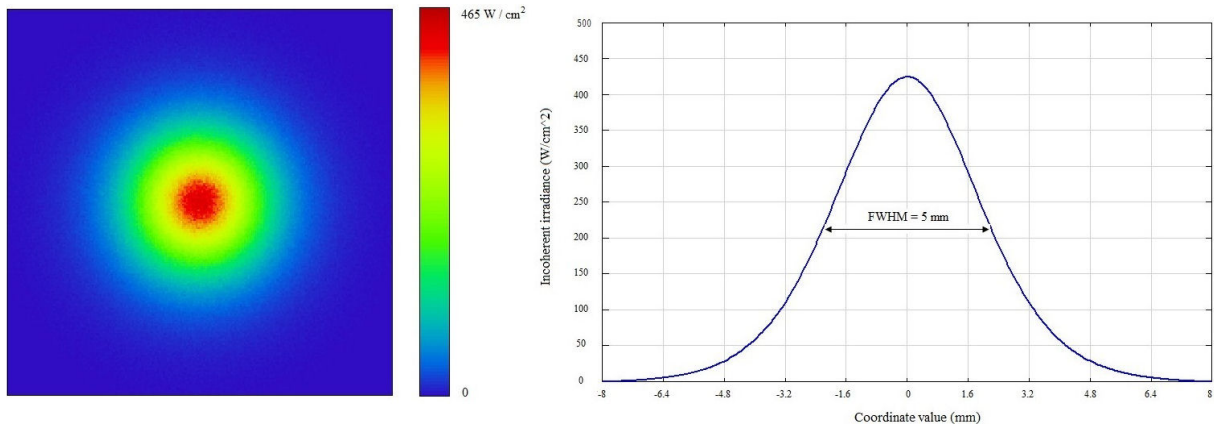


FIGURE 2. Exciting light distribution at the RAC focal point.

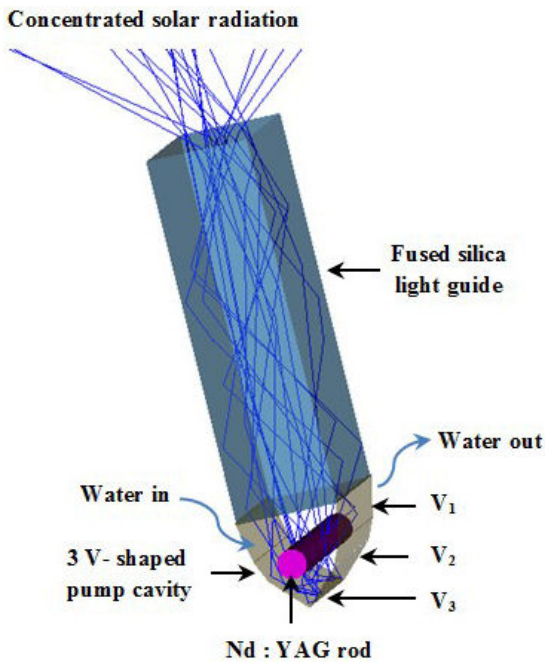


FIGURE 3. 3D design of the sunlight-pumped laser head for side exciting configuration.

3.3. Simulations with ZEMAX[®] and LASCAD[®] softwares

In the initial stage, a non-grooved Nd doped YAG laser rod of a diameter = 4.0 mm and length = 30 mm is placed within a 3 V-shaped excitation cavity. This rod is then side-excited using the concentrated sunlight by the ring-array concentrator, with the assistance of a silica light guide. The absorbed exciting power amounts to 48.92 W, and the optimized distribution of this power within the non-grooved Nd doped YAG rod, as determined by the ZEMAX[®] software, is illustrated in Fig. 4. Table III summarizes the dimensions of the head of the laser system elements.

The absorbed excitation power information from ZEMAX[®] software is after integrated in LASCAD[®] software. To get a maximum laser power in multi-mode regime, an optical resonator with a symmetrical configuration is considered, as indicated in Fig. 5.

Sunlight-pumped laser power of 11.18 W was computed adding to quality factors $M_x^2 = 33.92$ and $M_y^2 = 34.20$. The heat-load, the temperature, and the stress-intensity in the non-grooved Nd doped YAG rod, are exposed in Fig. 6.

In the second stage, the non-grooved Nd doped YAG rod is replaced with a grooved rod. To make the simulation more

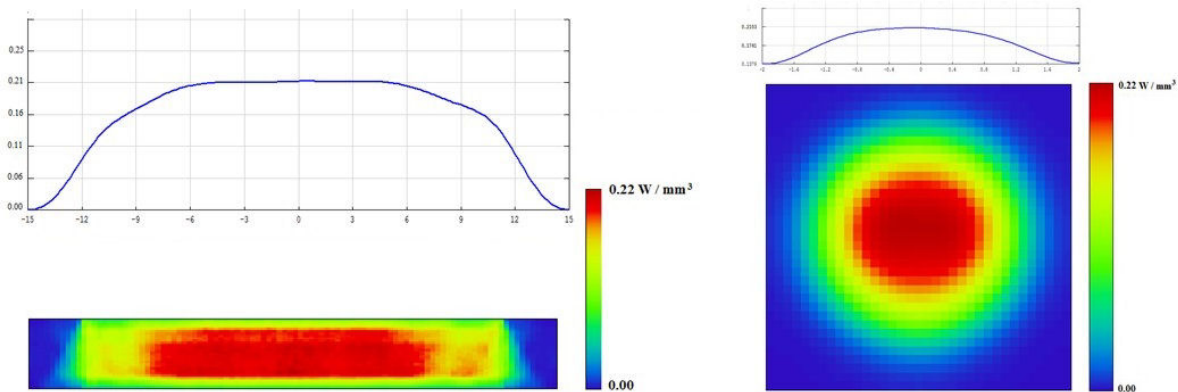


FIGURE 4. Absorbed excitation flux distribution along the longitudinal (left) and central (right) cross sections of the non-grooved Nd doped YAG rod.

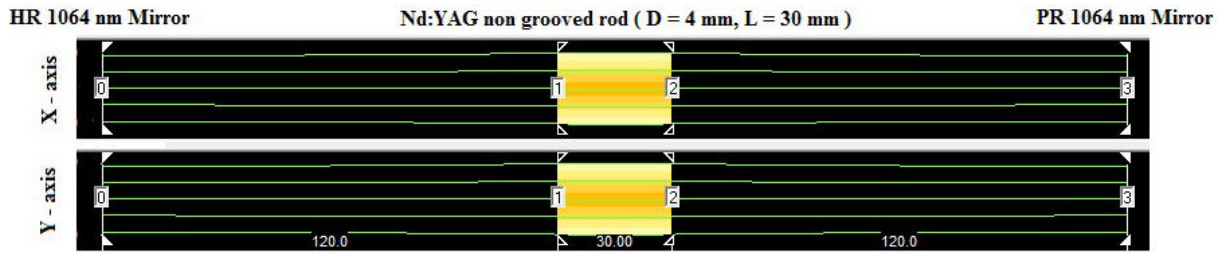


FIGURE 5. Symmetric laser-resonator for multi-mode sunlight-pumped laser operation by the non-grooved Nd doped YAG rod.

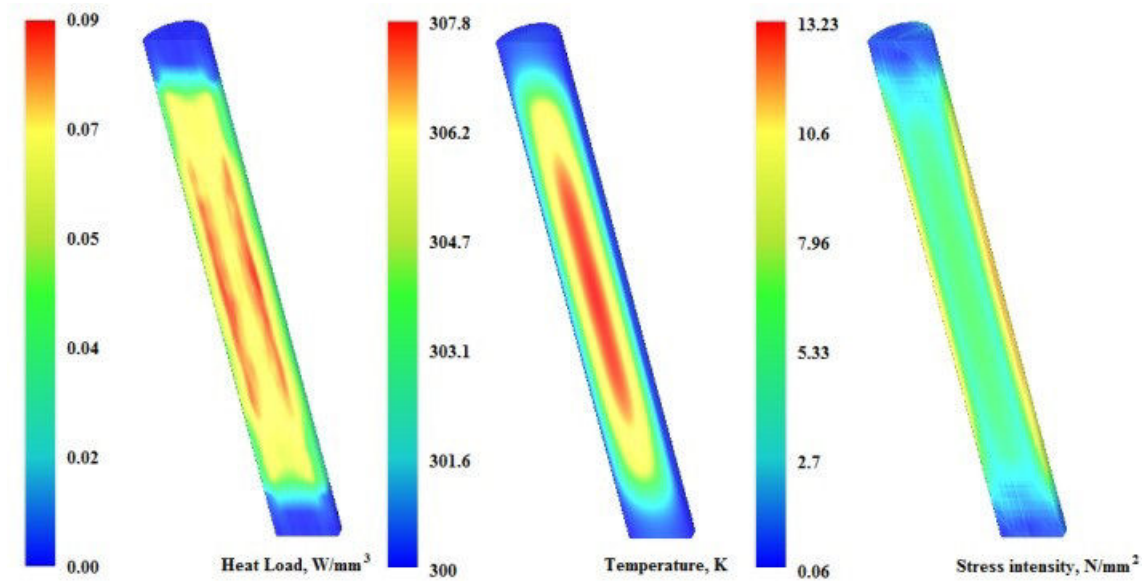


FIGURE 6. Computed heat-load, temperature, and stress-intensity distributions of the non-grooved Nd doped YAG rod.

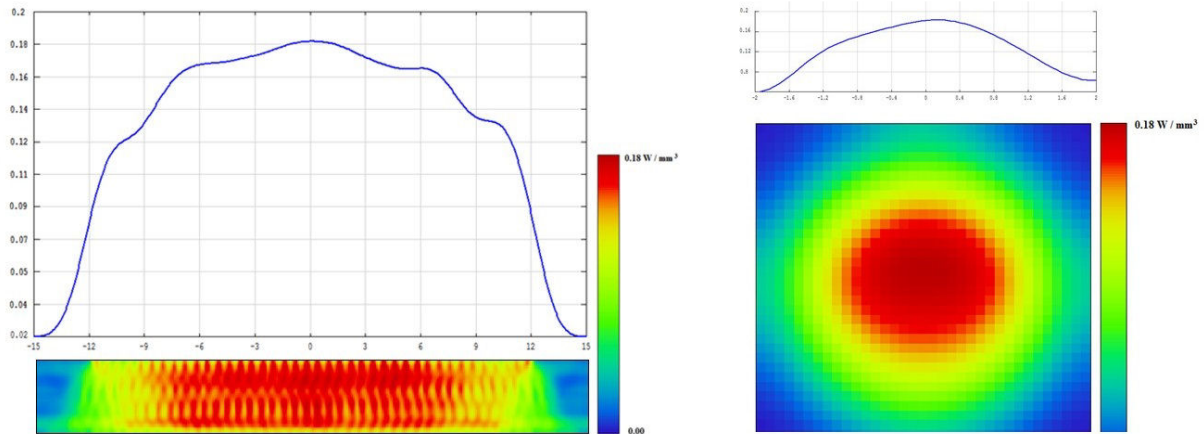


FIGURE 7. Absorbed excitation flux distribution along the longitudinal (left) and central (right) cross sections of the grooved Nd doped YAG rod.

realistic, a grooved Nd doped YAG rod from Union Optics Co., Ltd is employed in this study. Table IV summarizes the parameters characterizing the grooved rod. This substitution results in a maximum absorbed excitation power of 55.68 W.

3.4. End-exciting method

Despite the fact that end-exciting approaches are known for their high efficiency in sunlight-pumped laser systems, their

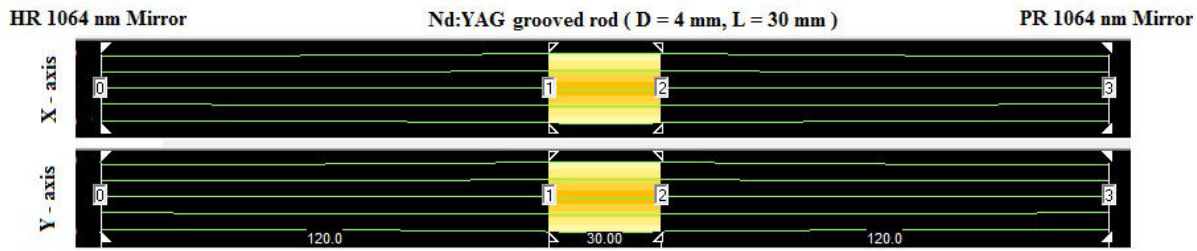


FIGURE 8. A symmetric laser resonator for multi-mode sunlight-pumped laser operation by the grooved Nd doped YAG rod.

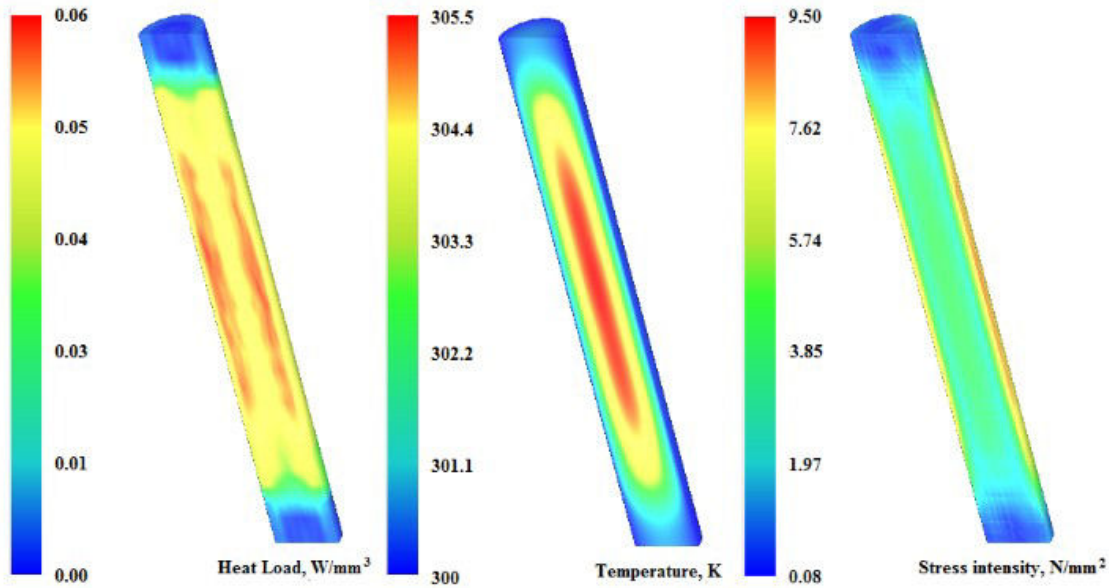


FIGURE 9. Computed heat load, temperature, and stress intensity distributions of the grooved Nd doped YAG rod.

TABLE IV. Parameters of the grooved-Nd doped YAG rod.

Grooved-Nd doped YAG rod	
Dimensions	Values
Diameter (mm)	4
Length (mm)	30
Grooved pitch (mm)	0.6
grooved depth (mm)	0.1

effectiveness is compromised by the negative impact of thermal loading. This is due to the non-regular distribution of the absorbed excitation light in these exciting methods.

3.5. Sunlight-pumped laser head

The head of the laser system is comprised of an aspheric lens of a fused-silica glass and an excitation cavity with a V-shaped configuration, where the Nd doped YAG rod is positioned. Figure 10 illustrates this arrangement of the laser head. Table V recapitulates the dimensions of the elements constituting the laser head.

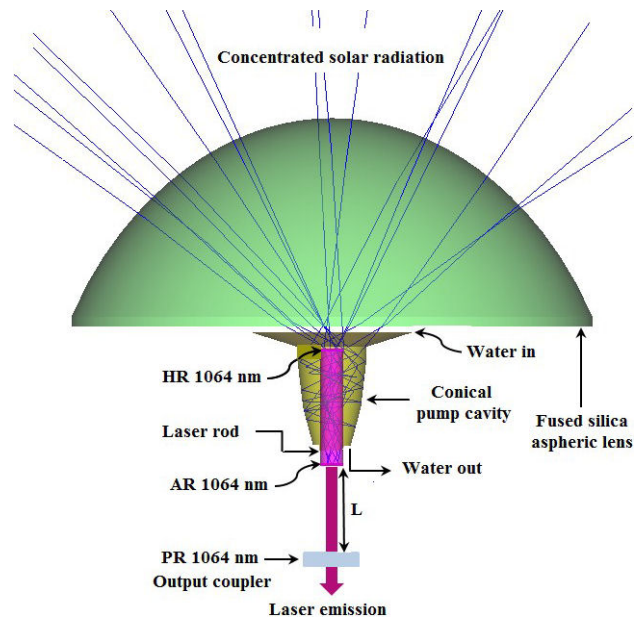


FIGURE 10. 3D design of the sunlight-pumped laser head, for end-exciting approach.

TABLE V. Dimensions of the laser head components.

Elements					
Aspheric lens of fused silica		Conical shaped excitation cavity		Nd doped YAG rod	
Dimensions	Values	Dimensions	Values	Dimensions	Values
Diameter (mm)	90	Input diameter (mm)	12	Diameter (mm)	4
Height (mm)	36	Output diameter (mm)	6		
Radius of curvature of front surface (mm)	50	Height (mm)	18	Length (mm)	20
Rear r^2 parameter	-0.003				

3.6. Examinations with ZEMAX© and LASCAD© software’s

In the first step, an end-side excitation method is employed with a non-grooved Nd doped YAG laser rod of measured diameter = 4 mm and length = 20 mm. The rod is placed inside a conical-shaped excitation cavity and subjected to focused sunlight at the ring-array concentrator focal point, facilitated by an aspheric lens of fused silica glass. One part of the concentrated radiation is directly focused onto the high reflection (HR 1064 nm) end face of the rod. The HR coating reflects the 1064 nm laser radiation within the resonator cavity but permits the passage of the other pumping wavelengths. The other part of the radiation is guided into the hollow conical cavity to ensure a multipass process, by the zigzag passage of the rays within the conical cavity to side pump the rod. Figure 11 displays the optimized distribution of the absorbed excitation power inside the non-grooved Nd: YAG rod as determined by the ZEMAX© software.

The optimized distribution of the absorbed excitation power inside the grooved Nd doped YAG rod, as determined by the ZEMAX© software is shown in Fig. 7. Figure 8 presents an optical resonator with a symmetrical configuration that leads to obtain a sunlight-pumped laser power of 12.71 W and the factors of the laser beam quality $M_x^2 = 32.42$, $M_y^2 = 32.66$. The heat-load, the temperature, and the stress-intensity inside the grooved-Nd doped YAG rod, are exposed in Fig. 9. The absorbed excitation power information obtained from ZEMAX© software is subsequently incorporated into LASCAD© software. To obtain the highest possible laser power in multimode operation, the upper end face of the rod is HR 1064 nm coated. The lower end face is antireflection (AR) coated for the same wavelength. The output coupler is partial reflection (PR) coated (PR at 1064 nm) and located 10 mm ($L = 10$ mm) away from the laser rod bottom AR face, as shown in Fig. 10.

The asymmetric optical laser resonator is hence formed by both HR 1064 nm reflector and PR 1064 nm output coupler, with 95% reflectivity and -1 m radius of curvature, as

TABLE VI. Results of the numerical study.

Side exciting		
	Non grooved rod	Grooved rod
Absorbed exciting power (W)	48.14	55.67
	An increase of 13.70%	
Laser power (W)	11.18	12.71
	An increase of 13.68%	
M_x^2	33.92	32.42
M_y^2	34.20	32.66
Heat load (W/mm ³)	0.09	0.06
Temperature (K)	307.8	305.5
Stress intensity (N/mm ²)	13.23	9.5
	A decrease of 28.2%	
End exciting		
	Non grooved rod	Grooved rod
Absorbed exciting power (W)	85.08	82.40
	A decrease of 3.15%	
Laser power (W)	23.96	22.85
	A decrease of 4.63%	
M_x^2	45.43	44.67
M_y^2	45.32	44.12
Heat load (W /mm ³)	0.6	0.63
Temperature (K)	344.3	344.1
Stress intensity (N/mm ²)	83.56	54.29
	A decrease of 35.03%	

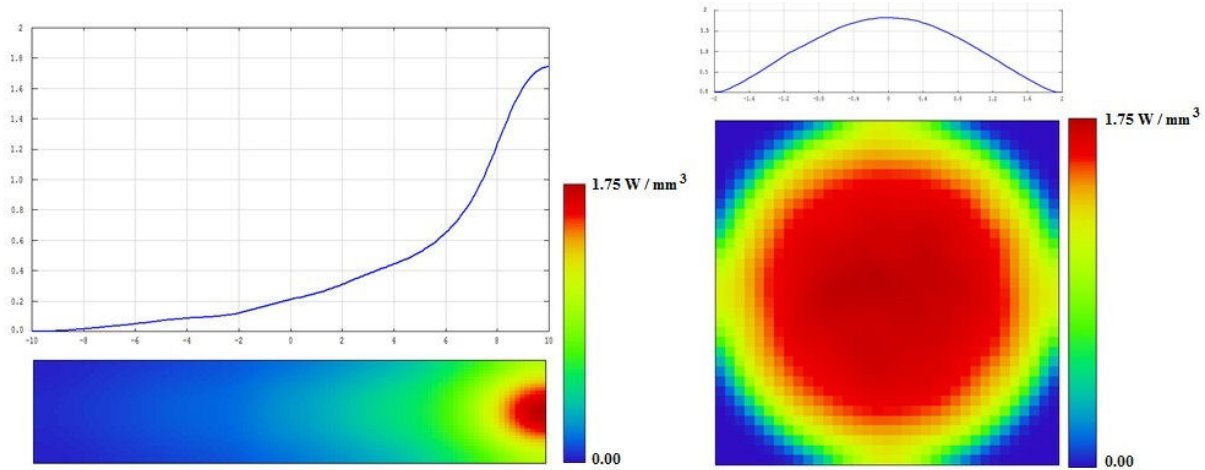


FIGURE 11. Absorbed excitation flux distribution along the longitudinal (left) and central (right) cross sections of the non-grooved Nd doped YAG rod.

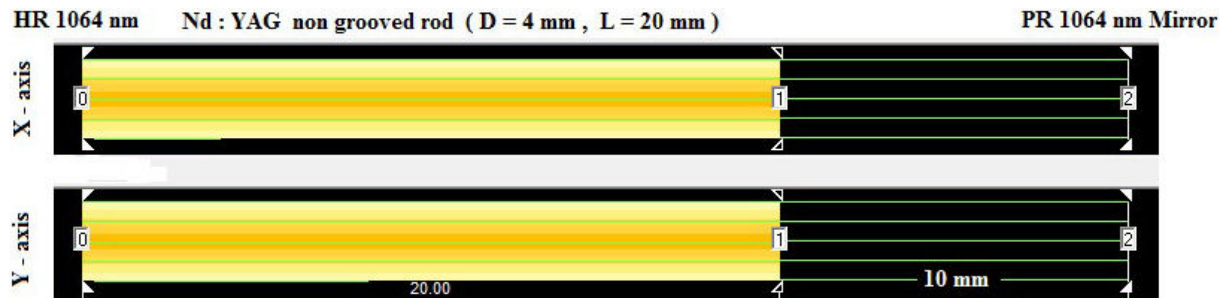


FIGURE 12. Asymmetric laser resonator for multi-mode sunlight-pumped laser operation by non-grooved Nd doped YAG rod.

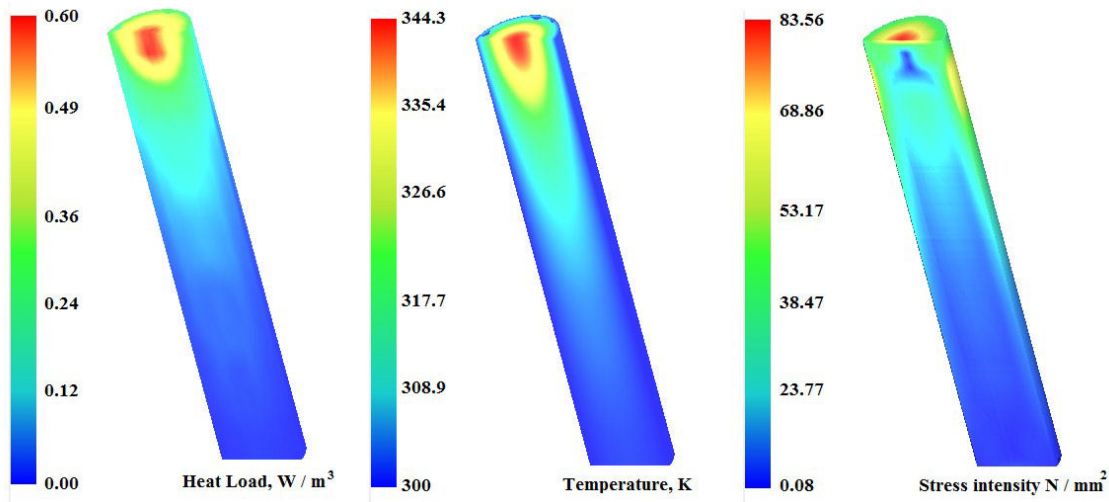


FIGURE 13. Computed heat load, temperature, and stress intensity distributions for the non-grooved Nd doped YAG rod.

depicted in Fig. 12. The calculations yield a sunlight-pumped laser power of 23.96 W, and the factors of the laser beam quality $M_x^2 = 45.43$ and $M_y^2 = 45.32$. The corresponding heat-load, temperature, and stress-intensity in the non-grooved Nd doped YAG rod are displayed in Fig. 13.

Next, a grooved Nd doped YAG laser rod is employed, which has a diameter = 4 mm and a length = 20 mm. The grooved rod features a grooved pitch = 0.6 mm and a grooved depth = 0.1 mm. By substituting the non-grooved rod with this grooved rod, an absorbed excitation power of 82.40 W is

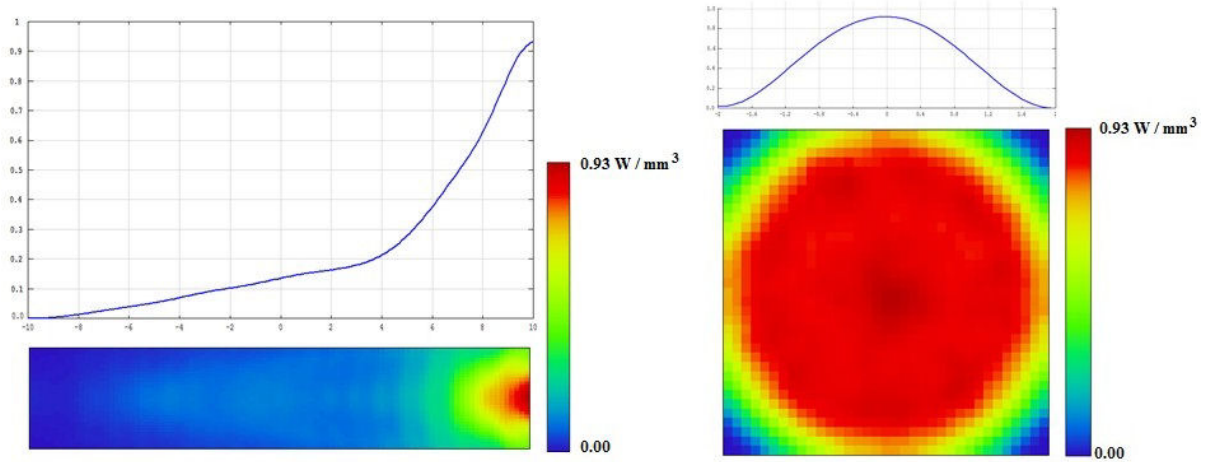


FIGURE 14. Absorbed excitation flux distribution along the longitudinal (left) and central (right) cross sections of the grooved Nd doped YAG rod.

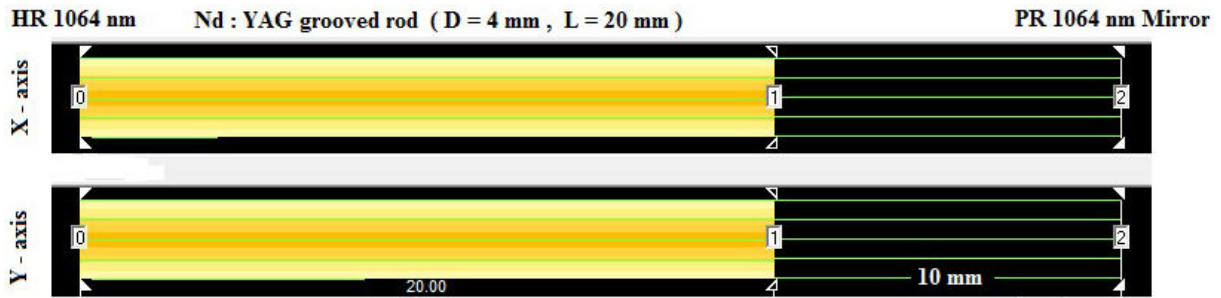


FIGURE 15. Asymmetric laser resonator for multi-mode sunlight-pumped laser operation by the grooved Nd doped YAG rod.

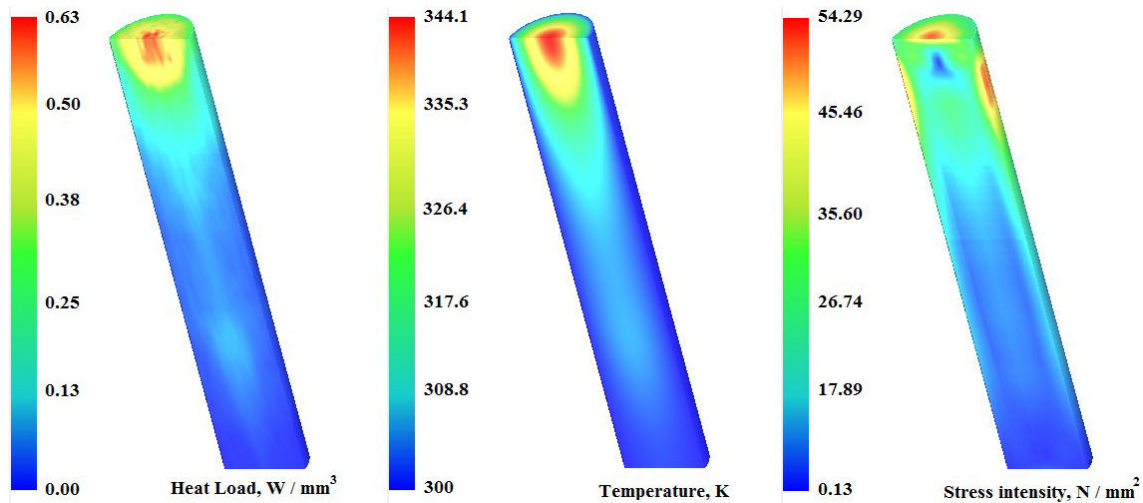


FIGURE 16. Computed heat load, temperature, and stress intensity distributions for the grooved Nd doped YAG rod.

achieved. The optimized distribution of the absorbed excitation power, determined using the ZEMAX[®] software, is presented in Fig. 14. Figure 15 presents an asymmetric optical resonator that leads to attain a sunlight-pumped laser power of 22.85 W, $M_x^2 = 44.67$, and $M_y^2 = 44.12$. Figure 16 exposes the heat load, temperature, and stress intensity in the grooved Nd doped YAG rod.

4. Discussions

Since the initial report on sunlight-pumped Nd doped YAG lasers in the early 1960s, various exciting designs have been introduced to advance the performance of sunlight-pumped

lasers. While end-side exciting approaches are known for their efficiency, they often suffer from thermal loading issues. On the other hand, side-exciting methods offer better laser beam quality by distributing the absorbed excitation light uniformly along the laser medium, effectively mitigating problems arising from thermal loading. However, side-pumping methods generally exhibit lower efficiency. One approach to enhance the efficiency of side-exciting systems is the use of grooved laser rods. V-shaped grooves on the rod's surface can minimize optical reflection losses, leading to improved efficiency and better heat dissipation through enhanced contact with the cooling liquid.

This, in turn, reduces stress intensity (as observed in this study, a decrease of 28.2%) and improves the laser beam quality. As known, in side-exciting method all the excitation light wraps the laser rod through its lateral surface, consequently, when this surface is grooved the excitation light absorption rises (meaning low-optical reflection losses) resulting in an increase of the output laser power (13.68% in this study). Hence, this pumping technique can be an attractive option for an efficient exciting system leading to a high laser beam quality.

In end-side-exciting approach, the majority of exciting light is compressed into the laser rod through its input-face, with a small portion laterally redirected by the excitation cavity to the rod's surface. As a result, the reduction of optical reflection losses through grooved surfaces has a weaker impact on end-exciting. The primary benefit of using grooved rods in end-exciting systems lies in improved heat dissipation through enhanced contact with the cooling liquid, leading to reduced stress intensity (as observed in this study, a decrease of 35.03%). While this reduces the thermal loading effect, it does not increase the absorbed exciting light into the laser rod

or result in higher laser power. Table VI provides a summary of the results obtained in this study.

These findings highlight the significance of the present study in initiating discussions regarding the practicality of employing grooved laser rods in end-side-exciting configurations.

5. Conclusion

A numerical investigation was conducted using ZEMAX[®] and LASCAD[®] software to survey the impact of grooving the Nd doped YAG rod on the performance of sunlight-pumped lasers in side-exciting and end-side-exciting techniques. The study examined how the grooved surface of the laser rod influenced the sunlight-pumped laser's performance. In the side-exciting method, the grooved rod demonstrated a 13.70% increase in sunlight-pumped laser power and a 28.2% reduction in stress intensity compared to the non-grooved rod. On the other hand, in the end-side-exciting scheme, the grooved rod primarily contributed to reducing thermal loading, resulting in a 35.03% reduction in stress intensity.

The grooved sides of the laser rod effectively minimized optical reflection losses, which played a main role in increasing the laser power in the side-exciting configuration. Based on the analysis of the obtained results, it is evident that the grooved laser rod offers a promising option for improving sunlight-pumped laser efficiencies in side-exciting configurations. Additionally, it is noteworthy that the side-exciting approach, in addition to generating high-quality laser beams, can serve as an efficient solar laser exciting system by utilizing the grooved laser rod.

-
1. Z. J. Kiss, H.R. Lewis, R. C. Duncan, Sun pumped continuous optical maser, *Appl. Phys. Lett.*, **2** (1963) 93, <https://doi.org/10.1063/1.1753794>.
 2. C. G. Young, A Sun-Pumped c. w. One-Watt Laser, *Opt.*, **5** (1966) 993, <https://doi.org/10.1364/AO.5.000993>.
 3. H. Arashi *et al.*, A Solar-Pumped c. w. 18 W Nd: YAG, Laser, *Jpn. J. Appl. Phys.*, **23** (1984) 1051, <https://doi.org/10.1143/JJAP.23.1051>.
 4. M. Weksler and J. Schwartz, Solar-pumped solid-state lasers, *IEEE J. Quantum Electron.*, **24** (1988) 1222, <https://doi.org/10.1109/3.247>.
 5. V. P. Vasylyev, O. G. Tovmachenko, and S. V. Vasylyev, Expected optical performances of novel type multi-element high-heat solar concentrators, in Proc. ASES Conf., (2002).
 6. M. Lando *et al.*, High-brightness solar-pumped Nd: YAG laser design, *Proc. SPIE* **2426** (1995) 478, <https://doi.org/10.1117/12.211229>.
 7. M. Lando, J. Kagan, B. Linyekin, V. Dobrusin, A solar-pumped Nd: YAG laser in the high collection efficiency regime, *Opt. Commun.*, **222** (2003) 371, [https://doi.org/10.1016/S0030-4018\(03\)01601-8](https://doi.org/10.1016/S0030-4018(03)01601-8).
 8. B. Zhao *et al.*, The study of active medium for solar-pumped solid-state lasers, *Acta Opt. Sin.*, **27** (2007) 1797.
 9. T. Saiki *et al.*, Oscillation property of rod type Nd/Cr: YAG ceramic lasers with quasi-solar pumping, in Conference on Lasers and Electro-Optics (CLEO) (IEEE), Paper No. CThT3, (2007), <https://doi.org/10.1109/CLEO.2007.4452870>.
 10. T. Yabe *et al.*, High efficiency and economical solar energy pumped laser with Fresnel lens and chromium co-doped laser medium, *Appl. Phys. Lett.* **90** (2007) 261120, <https://doi.org/10.1063/1.2753119>.
 11. T. Ohkubo, *et al.*, Solar-pumped 80 W laser irradiated by a Fresnel lens, *Optics Letters*, **34** (2009) 175, <https://doi.org/10.1364/OL.34.000175>.
 12. T. H. Dinh, T. Ohkubo, T. Yabe, H. Kuboyama, 120-watt continuous wave solar-pumped laser with a liquid light-guide lens and an Nd: YAG rod, *Opt. Lett.*, **37** (2012) 2670, <https://doi.org/10.1364/OL.37.002670>.

13. P. Xu *et al.*, High-efficiency solar-pumped laser with a grooved Nd: YAG rod, *Appl. Opt.* **53** (2014) 3941, <https://doi.org/10.1364/AO.53.003941>.
14. S. Payziyev and Kh. Makhmudov, A new approach in solar-to-laser power conversion based on the use of external solar spectrum frequency converters, *Journal of Renewable and Sustainable Energy*, **8** (2016) 015902, <https://doi.org/10.1063/1.4939505>.
15. S. Payziyev *et al.*, Simulation of a new solar Ce: Nd: YAG laser system, *Optik*, **156** (2018) 891, <https://doi.org/10.1016/j.ijleo.2017.12.071>.
16. S. Payziyev *et al.*, Luminescence sensitization properties of Ce: Nd: YAG materials for solar pumped lasers, *Opt. Commun.* **499** (2021) 127283, <https://doi.org/10.1016/j.optcom.2021.127283>.
17. R. Bouadjemine *et al.*, Stable TEM₀₀-mode Nd: YAG solar laser operation by a twisted fused silica light-guide, *Opt. Laser Tech.* **97** (2017) 1, <https://doi.org/10.1016/j.optlastec.2017.06.003>.
18. S. Mehellou *et al.*, Stable solar-pumped TEM₀₀-mode 1064nm laser emission by a monolithic fused silica twisted light guide, *Sol. Energy*, **155**, (2017) 1059, <https://doi.org/10.1016/j.solener.2017.07.048>.
19. S. Mehellou *et al.*, The Effects of the Pumping Configurations on TEM₀₀ Mode Nd: YAG Solar Laser Performance: a Review, *Brazilian Journal of Physics*, **52** (2022) 169, <https://doi.org/10.1007/s13538-022-01163-y>.
20. Z. Guan *et al.*, Low-threshold and high-efficiency solar-pumped laser with Fresnel lens and a grooved Nd: YAG rod, High-Power Lasers and Applications VIII, *Proc. of SPIE* **10016** (2016) 1001609, <https://doi.org/10.1117/12.2245281>.
21. Z. Guan *et al.*, 32.1 W/m² c. w. solar-pumped laser with a bonding Nd: YAG/YAG rod and a Fresnel lens, *Opt. Laser Technol.* **107** (2018) 158, <https://doi.org/10.1016/j.optlastec.2018.05.039>.
22. T. Masuda *et al.*, A fully planar solar pumped laser based on a luminescent solar collector, *Communications Physics* **3** (2020), <https://doi.org/10.1038/s42005-020-0326-2>.
23. D. Liang and J. Almeida, Highly efficient solar-pumped Nd: YAG laser, *Optics express*, **19** (2011) 26399, <https://doi.org/10.1364/OE.19.026399>.
24. D. Liang, J. Almeida, and E. Guillot, Side-pumped continuous-wave Cr: Nd: YAG ceramic solar laser, *Applied Physics B*, **111** (2013) 305, <https://doi.org/10.1007/s00340-013-5334-4>.
25. D. Liang and J. Almeida, Solar-pumped TEM₀₀ mode Nd: YAG laser, *Optics express*, **21** (2013) 25107, <https://doi.org/10.1364/OE.21.025107>.
26. D. Liang, J. Almeida, C. R. Vistas, and E. Guillot, Solar-pumped TEM₀₀ mode Nd: YAG laser by a heliostat-parabolic mirror system, *Solar Energy Materials and Solar Cells*, **134** (2015) 305, <https://doi.org/10.1016/j.solmat.2014.12.015>.
27. D. Liang *et al.*, High-efficiency solar-pumped TEM₀₀-mode Nd: YAG laser, *Solar Energy Materials and Solar Cells*, **145** (2016) 397, <https://doi.org/10.1016/j.solmat.2015.11.001>.
28. D. Liang, J. Almeida, and C. R. Vistas, 25W/m² collection efficiency solar pumped Nd: YAG laser by a heliostat-parabolic mirror system, *Appl. Opt.*, **55** (2016) 7712, <https://doi.org/10.1364/AO.55.007712>.
29. D. Liang, J. Almeida, C. R. Vistas, and E. Guillot, Solar-pumped Nd: YAG laser with 31.5 W/m² multimode and 7.9 W/m² TEM₀₀-mode collection efficiencies, *Sol. Energy Mater. Sol. Cells* **159** (2017) 435, <https://doi.org/10.1016/j.solmat.2016.09.048>.
30. D. Liang, C. R. Vistas, B. D. Tibúrcio, J. Almeida, Solar-pumped Cr: Nd: YAG ceramic laser with 6.7% slope efficiency, *Sol. Energy Mater. Sol. Cells*, **185** (2018) 75, <https://doi.org/10.1016/j.solmat.2018.05.020>.
31. D. Liang *et al.*, Side-pumped continuous-wave Nd: YAG solar laser with 5.4% slope efficiency, *Sol. Energy Mater. Sol. Cells*, **192** (2019) 147, <https://doi.org/10.1016/j.solmat.2018.12.029>.
32. D. Liang *et al.*, Simultaneous solar laser emissions from three Nd: YAG rods within a single pump cavity, *Solar Energy*, **199** (2020) 192, <https://doi.org/10.1016/j.solener.2020.02.027>.
33. D. Liang *et al.*, Seven-rod pumping approach for the most efficient production of TEM₀₀ mode solar laser power by a Fresnel lens, *Journal of solar energy engineering*, **143** (2021) 061004, <https://doi.org/10.1115/1.4051223>.
34. D. Liang *et al.*, Most efficient simultaneous solar laser emissions from three Ce: Nd: YAG rods within a single pump cavity, *Solar energy materials and solar cells*, **246** (2022) 111921, <https://doi.org/10.1016/j.solmat.2022.111921>.
35. D. Liang *et al.*, Solar-Pumped Lasers, Green Energy and Technology, Springer Nature Switzerland AG, (2023), <https://doi.org/10.1007/978-3-031-24785-9>.
36. J. Almeida, D. Liang, and E. Guillot, Improvement in solar-pumped Nd: YAG laser beam brightness, *Optics & Laser Technology*, **44** (2012) 2115, <https://doi.org/10.1016/j.optlastec.2012.03.017>.
37. J. Almeida, D. Liang, E. Guillot, and Y. Abdel-Hadi, A 40W c.w. Nd: YAG solar laser pumped through a heliostat: a parabolic mirror system, *Laser Physics*, **23** (2013) 065801, <https://doi.org/10.1088/1054-660X/23/6/065801>.
38. J. Almeida, D. Liang, C. R. Vistas, and E. Guillot, Highly efficient end-side-pumped Nd: YAG solar laser by a heliostat-parabolic mirror system, *Applied optics*, **54** (2015) 1970, <https://doi.org/10.1364/AO.54.001970>.
39. J. Almeida, D. Liang, R. Bouadjemine, and E. Guillot, 5.5W continuous-wave TEM₀₀-mode Nd: YAG solar laser by a light-guide/2V-shaped pump cavity, *Applied Physics B*, **121** (2015) 473, <https://doi.org/10.1007/s00340-015-6257-z>.
40. J. Almeida, D. Liang, and C. R. Vistas, A doughnut-shaped Nd: YAG solar laser beam, *Optics and Laser Technology*, **106** (2018) 1, <https://doi.org/10.1016/j.optlastec.2018.03.029>.

41. J. Almeida *et al.*, Numerical modeling of a four-rod pumping scheme for improving TEM₀₀-mode solar laser performance, *Journal of Photonics for Energy*, **9** (2019) 018001, <https://doi.org/10.1117/1.JPE.9.018001>.
42. J. Almeida *et al.*, Seven-rod pumping concept for simultaneous emission of seven TEM₀₀-mode solar laser beams, *Journal of Photonics for Energy*, **10** (2020) 038001, <https://doi.org/10.1117/1.JPE.10.038001>.
43. J. Almeida *et al.*, 40 W continuous wave Ce: Nd: YAG solar laser through a fused silica light guide, *Energies*, **15** (2022) 3998, <https://doi.org/10.3390/en15113998>.
44. C. R. Vistas, D. Liang, and J. Almeida, Solar-pumped TEM₀₀ mode laser simple design with a grooved Nd: YAG rod, *Solar Energy*, **122** (2015) 1325, <https://doi.org/10.1016/j.solener.2015.10.049>.
45. C. R. Vistas, D. Liang, J. Almeida, and E. Guillot, Solar-pumped TEM₀₀ mode laser simple design with a grooved Nd: YAG rod, *Optics Communications*, **366** (2016) 50, <https://doi.org/10.1016/j.optcom.2015.12.038>.
46. C. R. Vistas *et al.*, A doughnut-shaped Nd: YAG solar laser beam with 4.5 W/m² collection efficiency, *Solar Energy*, **182** (2019) 42, <https://doi.org/10.1016/j.solener.2019.02.030>.
47. C. R. Vistas *et al.*, Ce: Nd: YAG continuous-wave solar-pumped laser, *Optik*, **207** (2020) 163795, <https://doi.org/10.1016/j.ijleo.2019.163795>.
48. C. R. Vistas *et al.*, 32W TEM₀₀-Mode Side-Pumped Solar Laser Design, *Applied Solar Energy*, **56** (2020) 449, <https://doi.org/10.3103/S0003701X20060122>.
49. C. R. Vistas *et al.*, Ce: Nd: YAG side-pumped solar laser, *Journal of Photonics for Energy*, **11** (2021) 018001, <https://doi.org/10.1117/1.JPE.11.018001>.
50. C. R. Vistas *et al.*, Uniform and non-uniform pumping effect on Ce: Nd: YAG side-pumped solar laser output performance, *Energies*, **15** (2022) 3577, <https://doi.org/10.3390/en15103577>.
51. C. R. Vistas *et al.*, Fresnel Lens Solar Pumping for Uniform and Stable Emission of Six Sustainable Laser Beams under Non-Continuous Solar Tracking, *Sustainability*, **15** (2023) 8218, <https://doi.org/10.3390/su15108218>.
52. C. R. Vistas *et al.*, High Brightness Ce: Nd: YAG Solar Laser Pumping Approach with 22.9W/m² TEM₀₀-Mode Collection Efficiency, *Energies*, **16** (2023) 5143, <https://doi.org/10.3390/en16135143>.
53. D. Garcia *et al.*, A three-dimensional ring-array concentrator solar furnace, *Solar Energy*, **193** (2019) 915, <https://doi.org/10.1016/j.solener.2019.10.016>.
54. D. Garcia *et al.*, Analytical and numerical analysis of a ring-array concentrator, *International Journal of Energy Research*, **45** (2021) 15110, <https://doi.org/10.1002/er.6787>.
55. D. Garcia *et al.*, Elliptical-shaped Fresnel lens design through Gaussian source distribution, *Energies*, **15** (2022) 668, <https://doi.org/10.3390/en15020668>.
56. D. Garcia *et al.*, Ce: Nd: YAG solar laser with 4.5% solar-to-laser conversion efficiency, *Energies*, **15** (2022) 5292, <https://doi.org/10.3390/en15145292>.
57. D. Garcia *et al.*, Lowest-threshold solar laser operation under cloudy sky condition, *Renewable Energy*, **210** (2023) 127, <https://doi.org/10.1016/j.renene.2023.03.124>.
58. D. Garcia *et al.*, Efficient Production of Doughnut-Shaped Ce: Nd: YAG Solar Laser Beam, *Sustainability*, **15** (2023) 13761, <https://doi.org/10.3390/su151813761>.
59. R. Matos *et al.*, High-efficiency solar laser pumping by a modified ring-array concentrator, *Optics Communications*, **420** (2018) 6, <https://doi.org/10.1016/j.optcom.2018.03.027>.
60. B. D. Tibúrcio *et al.*, Improving solar-pumped laser efficiency by a ring-array concentrator, *J. Photon. Energy* **8** (2018) 018002, <https://doi.org/10.1117/1.JPE.8.018002>.
61. B. D. Tibúrcio *et al.*, Dual-rod pumping concept for TEM₀₀-mode solar lasers, *Applied Optics*, **58** (2019) 3438, <https://doi.org/10.1364/AO.58.003438>.
62. B. D. Tibúrcio *et al.*, Highly efficient side-pumped solar laser with enhanced tracking-error compensation capacity, *Optics Communications*, **460** (2020) 125156, <https://doi.org/10.1016/j.optcom.2019.125156>.
63. B. D. Tibúrcio *et al.*, Tracking error compensation capacity measurement of a dual-rod side-pumping solar laser, *Renewable Energy*, **195** (2022) 1253, <https://doi.org/10.1016/j.renene.2022.06.114>.
64. B. D. Tibúrcio *et al.*, Enhancing TEM₀₀-mode solar laser with beam merging and ring-array concentrator, *Journal of Solar Energy Engineering*, **144** (2022) 061005, <https://doi.org/10.1115/1.4054666>.
65. B. D. Tibúrcio *et al.*, Fresnel Lens Solar-Pumped Laser with Four Rods and Beam Merging Technique for Uniform and Stable Emission under Tracking Error Influence, *Energies*, **16** (2023) 4815, <https://doi.org/10.3390/en16124815>.
66. H. Costa *et al.*, Design of a multi-beam solar laser station for a megawatt solar furnace, *Optical Engineering*, **59** (2020) 086103, <https://doi.org/10.1117/1.OE.59.8.086103>.
67. H. Costa *et al.*, Quasi-Gaussian multi beam solar laser station for a megawatt solar furnace, *Journal of Solar Energies Research Updates*, **8** (2021) 11, <https://doi.org/10.31875/2410-4701.2021.08.02>.
68. H. Costa *et al.*, Zigzag multirod laser beam merging approach for brighter TEM₀₀-mode solar laser emission from a megawatt solar furnace, *Energies*, **14** (2021) 5437, <https://doi.org/10.3390/en14175437>.
69. H. Costa *et al.*, Multirod approach to enhance solar-to-laser conversion efficiency in the Odeillo solar furnace, *Journal of Photonics for Energy*, **12** (2022) 048001, <https://doi.org/10.3390/en14175437>.
70. H. Costa *et al.*, Seven-rod pumping concept for highly stable solar laser emission, *Energies*, **15** (2022) 9140, <https://doi.org/10.3390/en15239140>.

71. H. Costa *et al.*, Seven-grooved-rod, side-pumping concept for highly efficient TEM₀₀-mode solar laser emission through Fresnel lenses, *Photonics*, **10** (2023) 620, <https://doi.org/10.3390/photonics10060620>.
72. R. Boutaka *et al.*, A Compact Solar Laser Side-Pumping Scheme Using Four Off-Axis Parabolic Mirrors, *J. Russ. Laser Res.*, **42** (2021) 453, <https://doi.org/10.1007/s10946-021-09982-1>.
73. M. Catela *et al.*, Doughnut-shaped and top hat solar laser beams numerical analysis, *Energies*, **14** (2021) 7102, <https://doi.org/10.3390/en14217102>.
74. M. Catela *et al.*, Highly efficient four-rod pumping approach for the most stable solar laser emission, *Energies*, **13** (2022) 1670, <https://doi.org/10.3390/en13101670>.
75. M. Catela *et al.*, Stable emission of solar laser power under non-continuous solar tracking conditions, *Applied Optics*, **62** (2023) 2697, <https://doi.org/10.1364/AO.485158>.
76. M. Catela *et al.*, Solar laser pumping approach for both simultaneous and stable multi beam operation under tracking error condition, *Journal of Photonics for Energy*, **13** (2023) 028001, <https://doi.org/10.1117/1.JPE.13.028001>.
77. M. Catela *et al.*, Solar laser pumping approach for both simultaneous and stable multi beam operation under tracking error condition, *Journal of Photonics for Energy*, **13** (2023) 028001, <https://doi.org/10.1117/1.JPE.13.028001>.
78. M. Catela *et al.*, Stable emissions from a four-rod Nd: YAG solar laser with $\pm 0.5^\circ$ tracking error compensation capacity, *Photonics*, **10** (2023) 1047, <https://doi.org/10.3390/photonics10091047>.
79. S. Berwal *et al.*, A review on design modalities of solar-pumped solid-state laser, *Applied Surface Science Advances*, **12** (2022) 100348, <https://doi.org/10.1016/j.apsadv.2022.100348>.
80. Z. Cai *et al.*, Efficient $38.8W/m^2$ solar pumped laser with a Ce: Nd: YAG crystal and a Fresnel lens, *Optics Express*, **31** (2023) 1341, <https://doi.org/10.1364/OE.481590>.
81. W. Koechner, *Solid-State Laser Engineering*, 5th ed. (Springer-Verlag, Berlin, Heidelberg, New York, 1999).